# Numerical studies on soil-skirt roughness and sand plug impact in bearing capacity prediction of caisson foundations subjected to the uniaxial loads

Ghaseminejad, Vali; Barari, Amin; Rowshanzamir, Mohammad Ali

*Published in:*
Journal of Renewable and Sustainable Energy

*DOI (link to publication from Publisher):*
10.1063/1.5026698

*Publication date:*
2018

*Document Version*
Publisher's PDF, also known as Version of record

# Numerical studies on soil-skirt roughness and sand plug impact in bearing capacity prediction of caisson foundations subjected to the uniaxial loads

Vali Ghaseminejad, Amin Barari, and Mohammad Ali Rowshanzamir

Citation: Journal of Renewable and Sustainable Energy **10**, 053308 (2018); doi: 10.1063/1.5026698
View online: https://doi.org/10.1063/1.5026698
View Table of Contents: http://aip.scitation.org/toc/rse/10/5
Published by the American Institute of Physics

# Numerical studies on soil-skirt roughness and sand plug impact in bearing capacity prediction of caisson foundations subjected to the uniaxial loads

Vali Ghaseminejad,[1] Amin Barari,[2,a)] and Mohammad Ali Rowshanzamir[3]
[1]*Department of Civil Engineering, Isfahan (Khorasgan) Branch, Islamic Azad University, Isfahan, Iran*
[2]*Department of Civil Engineering, Aalborg University, Thomas Manns Vej 23, 9220 Aalborg Ø, Aalborg, Denmark*
[3]*Department of Civil Engineering, Isfahan University of Technology, Isfahan, Iran*

(Received 22 February 2018; accepted 10 September 2018; published online 12 October 2018)

Skirted foundations denoted as suction caissons are becoming an increasingly prevalent offshore foundation solution for either the oil and gas industry or renewable energy infrastructure. Their response to combined vertical, horizontal, and moment loading must be found to ensure their stability under harsh environmental conditions. As part of this process, knowledge of uniaxial capacities is required. Previous studies have neglected the effect of deformable ground by assuming that the soil within skirts behaves rigid during drained loading, but this assumption needs rigorous studies. A series of 3-D finite element analyses has been conducted to investigate directly how the skirt geometry, soil–skirt interface roughness, and deformable plug within the skirt compartment affect the drained skirted foundation capacity and depth factors under uniaxial loading. The results show that the foundation embedment, interface friction, and soil plug placed within the skirt significantly influence the accompanying mechanisms occurring at failure and therefore the uniaxial capacities. The finite element analyses under uniaxial loads are performed for the rough and smooth interface assumptions, to show how the roughness interface influences the ultimate bearing capacities and depth factors and the corresponding failure mechanisms in different soil profiles. *Published by AIP Publishing.* https://doi.org/10.1063/1.5026698

## I. INTRODUCTION

Some applications of foundation systems for offshore wind turbines involve gravity, monopile, tripod, jacket, and floating foundations depending on the seabed conditions and water depth. Suction Caissons with skirt length to diameter ratios $L/D > 1$ have been originally used as the suitable engineering solution for the offshore oil and gas industry. In an offshore wind turbine foundations, load conditions are inherently complex. Vertical loads involve the self-weight of the wind turbine structure, which transfer a small load to the bucket foundation with respect to the vertical bearing capacity when compared to the other uniaxial loads (i.e., horizontal and moment) acting on the wind turbine (Foglia *et al.*, 2013). Large horizontal forces and bending moments may endanger the serviceability of the bucket foundation, and thus, using suitable footing constructions, the harsh loads must be economically and safely transferred to the seabed. An alternative foundation option to other solutions in the next generation of offshore wind turbines is the bucket foundation with aspect ratios $L/D \leq 1$ that can be used as mono-bucket or tripod foundations. Recent evaluations have proven that bucket foundations may be used as support structures, owing to their simplicity of installation and construction, reliability, economic advantages, and repetitive usability (Houlsby *et al.*, 2005; Barari and

a)Author to whom correspondence should be addressed: ab@civil.aau.dk and abarari@vt.edu

Ibsen 2012, 2017; Zhang *et al*., 2014; Vulpe 2015; Liu *et al*., 2015; Barari *et al*., 2017; and Wang *et al*., 2017). To improve the fixity of the offshore structures under severe loading conditions, bucket foundations are fitted with hollow and large diameter tubular skirts, closed at the top and open at the bottom. They are embedded into the subsoil under their deadweight, confining a soil plug, and lowered onto the seabed by applying a differential suction pressure inside the skirt compartment until full penetration is achieved (Ibsen, 2008). In fact, the plug confined inside the circumferential skirts of skirted foundations opposes to a solid body and behaves like a deformable plug (Barari and Ibsen, 2012).

It is therefore important to distinguish between the behavior of embedded and skirted foundations. While investigation of bearing capacity of shallow foundations has typically considered fully solid concepts (e.g., Salgado *et al*., 2004 and Gourvenec, 2008), the bearing behavior, failure mechanisms, and stiffness of skirted foundation have received considerable attention recently (Yun and Bransby, 2007; Mana *et al*., 2012; Liu *et al*., 2017; Wang *et al*., 2017; Jalbi *et al*., 2018; and Zou *et al*., 2018).

Bucket foundations are subjected to combined loading, and thus, combinations of moment, vertical, and horizontal loads resulting from the superstructure and environmental conditions (i.e., waves, wind and current) acting on the bucket foundation must be investigated.

Prediction of uniaxial bearing capacities is one of the important issues in order to provide better understanding regarding the effect of pure loading types before the estimation of combined capacities and load interaction diagrams. Uniaxial bearing capacities can be used for the determination of failure envelopes in specific states under combined loads (i.e., combined horizontal and moment loads) (Larsen *et al*., 2013; Achmus *et al*., 2013; and Ibsen *et al*., 2014a, 2014b).

Although the bearing capacity behavior of the bucket foundation may consist of complex load distribution in three-dimensional space along the normal stresses on the skirts and shear stresses at the bucket circumference, traditional design guidelines still employ simple soil reaction concepts used for piles. During the last few decades, conventional design approaches for determining the bearing capacity of offshore shallow footings (i.e. DNV 1992, API 2002 and ISO 2003) have been gradually replaced by the use of interaction diagrams in the two and three-dimensional load spaces. Hence, the main objective of recent studies has been to overcome the drawbacks of conventional bearing capacity theories in favor of a new framework capable of capturing the effects of foundation geometry, non-linearity of soil, load eccentricity, embedment, and load inclination, which oppose the consideration of separate modification factors.

The work-hardening plasticity theory such as Macro-Element Models for soil-foundation interaction has been employed by a number of researchers in the field of offshore engineering, which account for describing the baring capacity under combined vertical, horizontal, and moment loading (Gourvenec and Randolph 2002, 2003; Bransby and Yun 2009; Gerolymos *et al*., 2012; Barari and Ibsen 2012; Bienen *et al*., 2012; Larsen *et al*., 2013; Ibsen *et al*., 2014a, 2014b, 2015; and Zafeirakos and Gerolymos 2016).

Regarding the soil-foundation interface, Bransby and Randolph (1998), Gourvenec and Randolph (2002, 2003), and Gourvenec (2007), among others considered rough behavior with a full contact at the interface between soil and foundation, resulting in the generation of optimistic bearing capacities.

There are some research works in the literature, which refer exclusively to the derivation of uniaxial capacities in skirted footings. As an example, Park *et al*. (2016) evaluated the bearing capacity and derived unique vertical load transfer characteristics of bucket foundations installed in the sand using the two-dimensional axisymmetric finite element analyses. They highlighted the occurrence of the Arching phenomenon between the skirts and confined soil during vertical displacement, which causes the failure surface to widen due to additional vertical stress distributed on the soils surrounding the bucket.

Moreover, due to the convoluted interaction of the effective parameters, such as foundation dimensions, aspect ratio, relative density, and interface roughness, few studies develop simple closed-form solutions which refer exclusively to skirted footings for use in the primary design process.

Estimation of the bearing capacity for skirted footings under uniaxial loads in varying sand profiles and interface roughness is missing from the literature, and this is what the present study directs. The aim of the current research is to evaluate the effect of aspect ratios and sand relative densities on the pure bearing capacity of bucket foundations with smooth and rough soil–skirt interfaces in saturated sands.

In the above context, two soil-skirt interface friction ratios (i.e., $R_{\text{inter}} = 0.7$ corresponding to the rough interface condition and $R_{\text{inter}} \sim 0$ reflecting the smooth interface condition) have been deliberately chosen in order to highlight the possible impacts of imperfect conditions. These assumptions reflect the maximum shear resistance that may be mobilized at the soil-foundation interface.

On the basis of 3D numerical analyses, explicit approximate expressions were derived as a function of embedment ratio, enabling the prediction of uniaxial bearing capacities and depth factors with varying soil profiles and soil-skirt roughness interfaces for comparison purposes. Meanwhile, the kinematic failure mechanisms were subsequently represented. Analyses were performed by loading the suction buckets in a way that allowed the bucket to move freely, similar to the footings in offshore sites (Fig. 1).

## II. FINITE ELEMENT MODEL

The study herein presents a campaign to examine the performance of skirted foundations by a three-dimensional finite element framework in order to further utilize it in the scope of a parametric study. Plaxis 3D Foundation software package (2005) was employed to model the bucket foundations. External boundaries were set sufficiently remote to reach the acceptable accuracy of the results. Hence, the behavior of the bucket foundation is not significantly influenced by the boundary conditions. The length of the finite-element mesh boundary was set to 6 times the bucket diameter, and the bottom boundary of the model was extended 3 times the bucket skirt length. The elements used in the 3D finite element calculations were 15 node triangular elements.

The roughness of the interaction between the bucket interface and soil was defined choosing a suitable value for the strength reduction factor in the interface ($R_{\text{int}} = (\tan\delta/\tan\phi)$, where $\delta$ is the friction angle between soil and skirt and $\varphi$ is the internal friction angle of the soil), which would relate the interface strength to the soil strength which is considered as 0.7. It should be noted that the assumption of a full contact between the soil and the foundation (i.e., fully rough interface) may not be accurate, which leads to an overestimated prediction of the bearing capacity owing to uplifting and tension. Finite element analyses were carried out on different interface assumptions (i.e., smooth and rough) to show how each of them would influence failure mechanisms produced under uniaxial loads. Figure 2 shows the finite element mesh with geometrical properties, which was adopted in the present study.

Caisson foundations embedded in different sand profiles (loose, medium, and dense sands with relative densities of 30%, 55%, and 80%, respectively), with diameter $D = 12$ m, 16 m

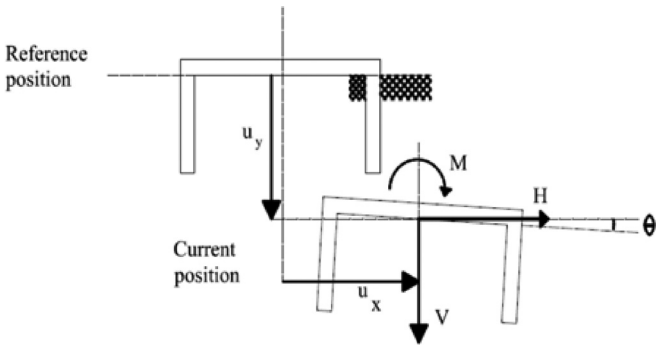


FIG. 1. Sign convention for loads and displacements.

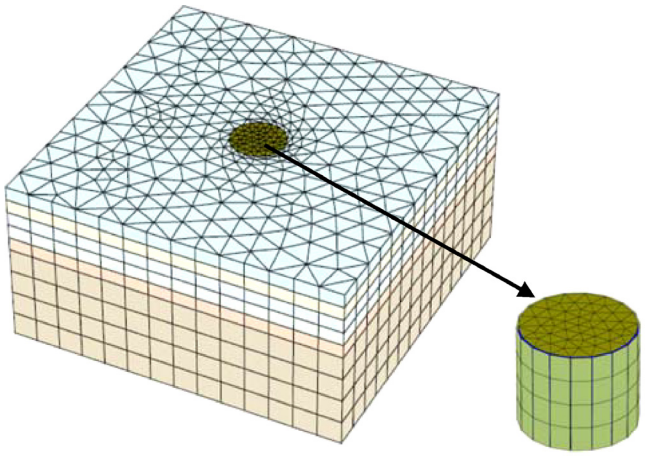

FIG. 2. A Schematic view of the finite element mesh used in the analyses.

and different aspect ratios ($L/D = 0$, 0.25, 0.5, 0.75, 1), were studied. In the analyses, the deformation properties of the bucket which is composed of steel materials with a modulus of elasticity $E = 210$ GPa and Poisson's ratio $\nu = 0.2$ were considered. The submerged unit weight of the steel used for the bucket body was set to $\gamma' = 68\,\text{kN/m}^3$. A top plate thickness of $t_L = 0.10$ m, a unit weight of $\gamma' = 77\,\text{kN/m}^3$, and a very large modulus of elasticity of $E = 1 \times 10^9$ GPa were selected for the bucket lid.

Pure moment was applied by adding opposite direction couple loads with eccentricity of h ($M = H.h$) to the alignment of the reference point at the center of the bucket lid. Pure horizontal, vertical, and moment loads were applied separately on the bucket lid and increased gradually until the pure bearing capacity of the bucket foundation was reached. The bearing capacity was obtained at the intersection point of two tangential lines along the initial and latter portions of the load-deformation curve for all pure vertical, horizontal, and moment loads.

To simulate non-linear soil response, the stress-dependency of the oedometric modulus of elasticity was implemented through the following expression (Achmus *et al.*, 2013):

$$E_s = \kappa.\sigma_{at}.\left(\frac{\sigma_m}{\sigma_{at}}\right)^{\lambda}, \tag{1}$$

where $\sigma_m$ is the current mean principle stress in the considered soil element and $\sigma_{at} = 100\,\text{kN/m}^2$ is the reference stress. Parameters $\kappa$ and $\lambda$ are related to soil stiffness in the reference stress state. Table I shows the parameters of the material used for sands with different properties (Houlsby *et al.*, 2005 and Achmus *et al.*, 2013).

## III. VALIDATION OF THE NUMERICAL MODEL

In this study, numerical analyses were calibrated with large-scale field test data in Frederikshavn presented in the literature (Houlsby *et al.*, 2005). In the test, the model bucket foundation with a diameter of $D = 2$ m, a skirt length of $L = 2$ m, and a skirt thickness of $t_s = 12$ mm located in a very dense fine sand was subjected to the campaign of lateral loads and moments. The test was carried out with a horizontal loading eccentricity of $h = 17.4$ m. The vertical load during the test was considered $V = 37.3$ kN. The thickness of the lid as well as material properties of bucket was modeled as presented in Sec. II. The numerical analysis is seen to agree well with the test data obtained by Houlsby *et al.* (2005), as shown in Fig. 3(a). In the figure, $M$, $R$, and $\theta$ are the moment, radius, and rotation of the bucket, respectively.

To further investigate, the finite element (FE) model of skirted footing was validated with the results of analysis obtained by Achmus *et al.* (2013). For comparison, a bucket with $D = 12$ m, a skirt length of $L = 9$ m ($L/D = 0.75$), and a skirt thickness of $t_s = 3$ cm under a loading

TABLE I. Material properties used in the numerical analysis.

| Property | Loose sand | Medium dense sand | Dense sand | Unit |
|---|---|---|---|---|
| Submerged unit weight ($\tilde{a}'$) | 7 | 9 | 11 | [kN/m$^3$] |
| Oedometric stiffness parameter ($\hat{e}$) | 300 | 400 | 600 | [−] |
| Oedometric stiffness parameter ($\ddot{e}$) | 0.65 | 0.6 | 0.55 | [−] |
| Poisson's ratio ($\acute{\imath}$) | 0.25 | 0.25 | 0.25 | [−] |
| Internal friction angle ($\ddot{o}'$) | 30 | 35 | 40 | [°] |
| Dilation angle ($\phi$) | 2.5 | 5 | 10 | [°] |

eccentricity of $h = 100$ m and a vertical load of $V = 10$ MN was analyzed. Dense soil parameters are tabulated in Table I. Figure 3(b) presents good agreement between the literature and the current work.

## IV. VERTICAL CAPACITY

Vertical loads on bucket foundations are derived from their self-weight as well as the shaft. Byrne and Houlsby (1999) illustrated that the influence of the skirt friction on the uniaxial bearing capacity of skirted foundation is negligible for small scale bucket foundations tested in the laboratory on dense sand and is not sensitive to slight changes in the interface roughness.

Figure 4 shows the view of failure mechanisms under pure vertical loading at $D = 16$ m for $L/D = 0.25$ and 1 at smooth and rough interfaces. Deformation mechanisms are known as total displacement shadings that accompany failures in pure vertical loads. Shadings of the plastic deformation accompanying bucket failure indicate that symmetric punching failure initially illustrated in Vesic (1963, 1973) is a dominant mechanism for skirted footings with $L/D = 1$. Meanwhile, a closer inspection highlights the dominant mechanism of local shear type for the response of buckets with an aspect ratio of 0.25, irrespective of the $\mu$ coefficient.

To account for the remarkable discrepancy in the dominant failure mechanism represented by displacement vectors and plastic strain distribution of skirted footings with varying embedment ratios, Fig. 4 displays the confined (i.e., constrained) soil plug in the skirt compartment which acts as a rigid body for the rough-interface bucket foundation at an embedment ratio of $L/D = 1$ in which the shear band forms outside the skirt compartment. Increasing the relative density and skirt dependence on the normal stresses yields much greater bearing capacity than weaker sands.

It can also be observed that in the case of the caissons with a rough soil-skirt interface, a significant part of the loading is transferred to the soil inside the sidewalls of the footing, mobilizing the greater shear resistance of the surrounding soil, especially for the higher aspect ratios.

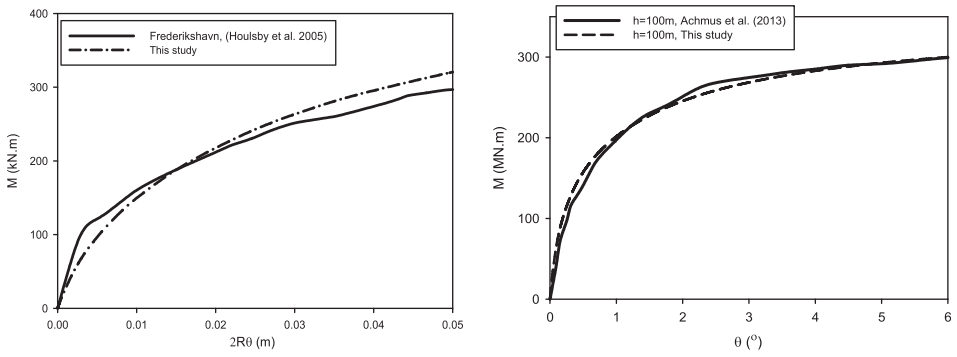


(a) (b)

FIG. 3. Comparison results of finite element with (a) field test (Houlsby *et al.*, 2005) and (b) numerical results (Achmus *et al.*, 2013).

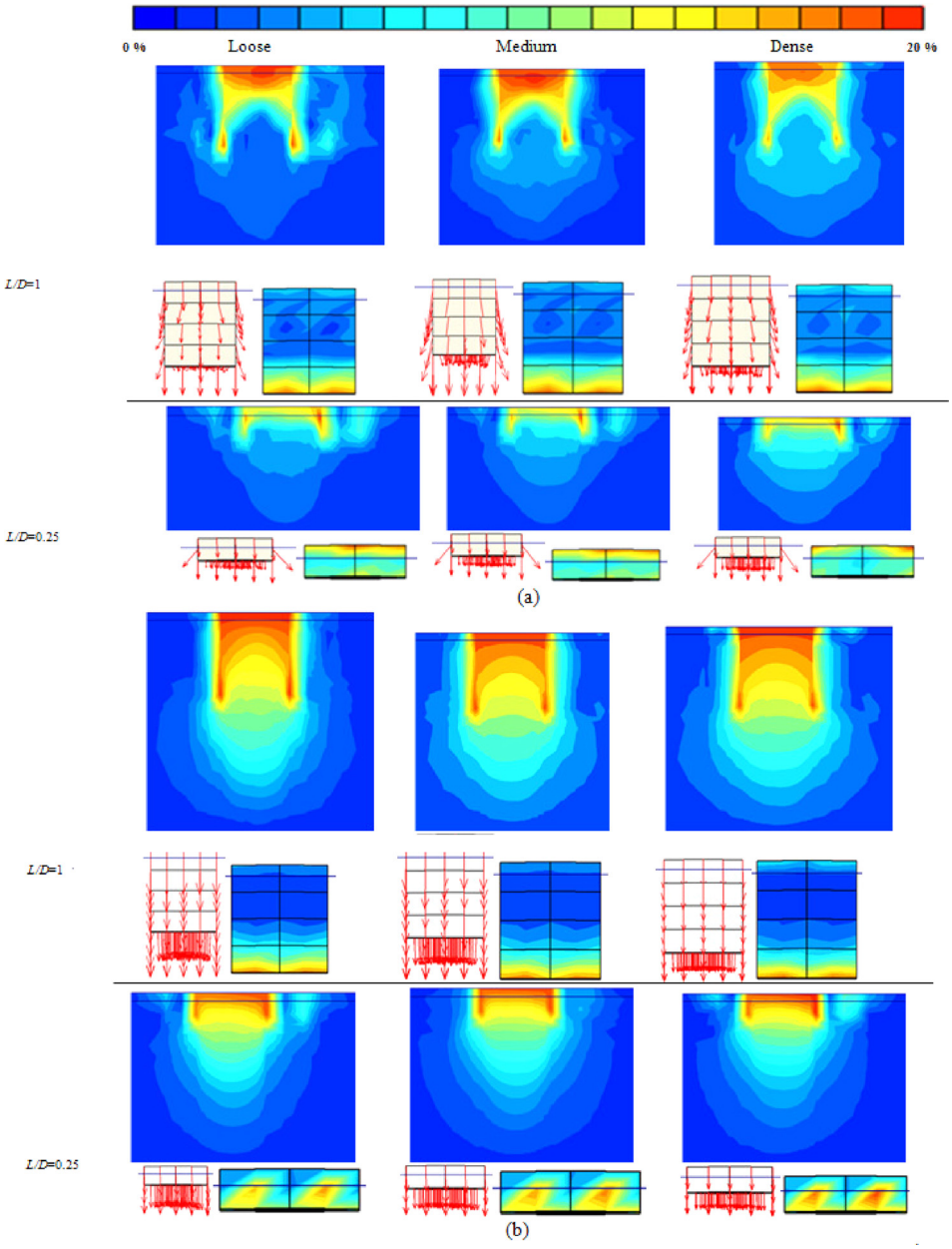


FIG. 4. Comparison of the failure mechanisms under pure vertical loading (a) smooth interface and (b) rough interface.

Concerning smooth interfaces, sidewalls play almost no role in the load-carrying capacity of the caisson against vertical loading. Moreover, the shear strength in the loose sand deposit is expectedly lower than that in the medium-dense and dense sands, which implies that the bigger plastic shear zones are created. In what follows, Fig. 5 shows pure vertical bearing capacities versus $L/D$ curves in a variety of soil profiles and interface roughness.

At large aspect ratios, bucket foundations in different sands represented higher vertical bearing capacities since their sidewalls involved higher shear strengths. In fact, surface sands trapped within the skirt enhanced vertical bearing capacities in which applied loads moved down to harder underlying layers.

Figure 6 and Table II express the pure vertical capacity depth factors ($d_{cv} = V_{ult(L/D)}/V_{ult(L/D=0)}$) with respect to the soil-skirt roughness. However, the results of the present study showed that a linear function may be considered in the $d_{cV}$-$L/D$ curve at different diameters and sand types.

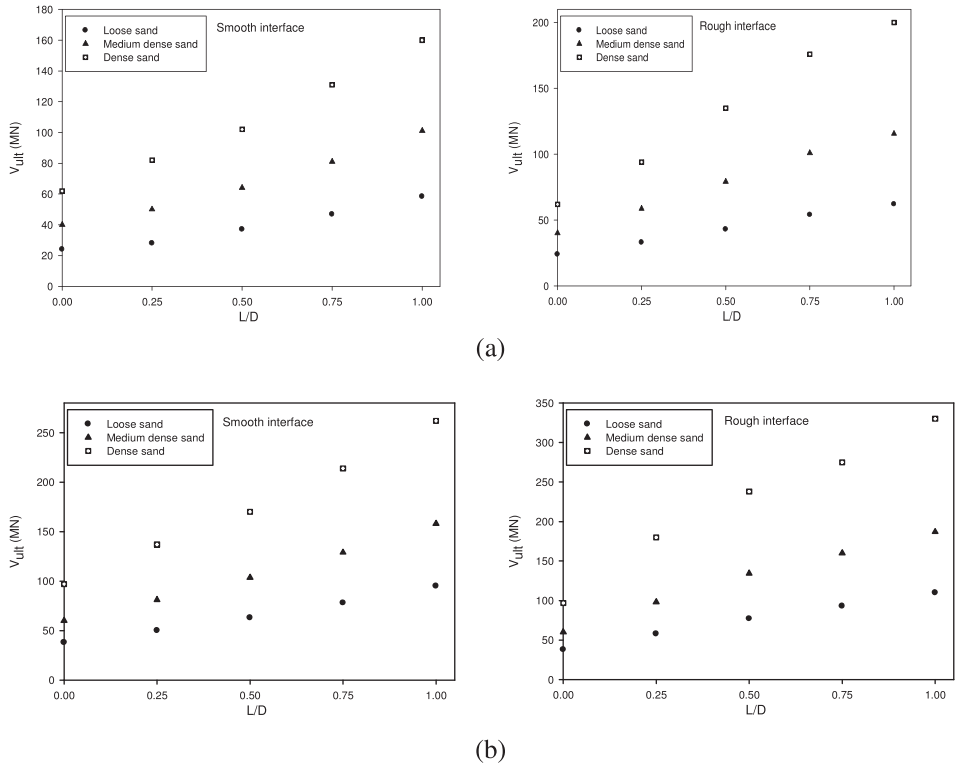


FIG. 5. Pure vertical bearing capacities versus aspect ratios with varying sand profiles for smooth and rough interfaces, (a) $D = 12$ m and (b) $D = 16$ m.

Due to limited experiments reported in the context of behavior of skirted foundations, only a few relationships have been presented for the bearing capacity depth factor.

An investigation into the drained behavior of bucket foundations in very dense and dry sand subjected to the vertical loads was conducted by Byrne and Houlsby (1999). The study suggested a linear relationship linking the bearing strength of a skirted footing, $V_{peak}$, with the corresponding surface one, $V_0$, as follows:

$$\frac{V_{peak}}{V_0} = 1 + 0.89\left(\frac{L}{D}\right). \tag{2}$$

The bearing capacity criteria adopted in their research utilized the friction angle of 46° and have eliminated the soil-skirt friction. Later on, Ibsen *et al.* (2012) rewrote the normalized bearing capacity of bucket foundations in cohesionless soil with a friction angle of 48°as follows:

$$\frac{V_{peak}}{V_0} = 1 + 2.1\left(\frac{L}{D}\right). \tag{3}$$

It was pointed out that the equation may only be valid in small scale tests performed by Byrne and Houlsby (1999) (Barari *et al.*, 2017). Unlike Byrne and Houlsby (1999), a linear relationship between the vertical bearing capacity depth factor and the aspect ratio in saturated sand assuming a mean friction angle of 42° was afterwards proposed in Barari *et al.* (2017)

$$\frac{V_{peak}}{V_0} = 1 + 2.9\left(\frac{L}{D}\right). \tag{4}$$

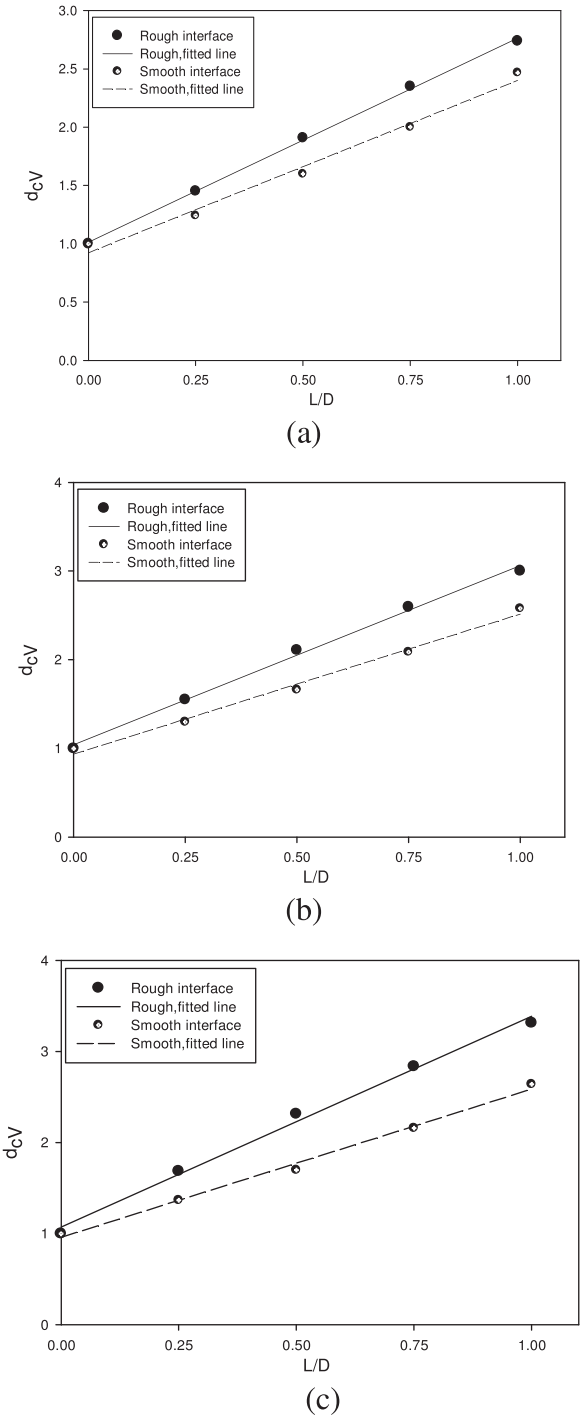


FIG. 6. Comparison of pure vertical capacity depth factors between smooth and rough bucket foundations, (a) loose sand, (b) medium sand, and (c) dense sand.

## V. HORIZONTAL CAPACITY

Figure 7 shows the view of incremental displacement contours and vectors under pure horizontal loading at $D = 16$ m for $L/D = 0.25$, 1 at smooth and rough interfaces.

In pure horizontal loading, the coupling between the horizontal and rotational degrees of freedom played an important role. As such, failure shape also altered from a purely horizontal

TABLE II. Depth factor relationships.

| Soil-skirt interface parameters | Soil properties | Smooth | Rough |
|---|---|---|---|
| $d_{cV}$ | Loose | $d_{cV} = 1 + 1.37\left(\frac{L}{D}\right)$ | $d_{cV} = 1 + 1.77\left(\frac{L}{D}\right)$ |
| | Medium | $d_{cV} = 1 + 1.50\left(\frac{L}{D}\right)$ | $d_{cV} = 1 + 2.07\left(\frac{L}{D}\right)$ |
| | Dense | $d_{cV} = 1 + 1.58\left(\frac{L}{D}\right)$ | $d_{cV} = 1 + 2.41\left(\frac{L}{D}\right)$ |
| $d_{\mathrm{cH}}$ | Loose | $d_{cH} = 1 + 5.77\left(\frac{L}{D}\right)$ | $d_{cH} = 1 + 8.36\left(\frac{L}{D}\right)$ |
| | Medium | $d_{cH} = 1 + 6.03\left(\frac{L}{D}\right)$ | $d_{cH} = 1 + 9.53\left(\frac{L}{D}\right)$ |
| | Dense | $d_{cH} = 1 + 6.28\left(\frac{L}{D}\right)$ | $d_{cH} = 1 + 10.34\left(\frac{L}{D}\right)$ |
| $d_{\mathrm{cM}}$ | Loose | $d_{cM} = 1 + 3.04\left(\frac{L}{D}\right) + 2.7\left(\frac{L}{D}\right)^2$ | $d_{cM} = 1 + 2.22\left(\frac{L}{D}\right) + 7.22\left(\frac{L}{D}\right)^2$ |
| | Medium | $d_{cM} = 1 + 3.26\left(\frac{L}{D}\right) + 3.33\left(\frac{L}{D}\right)^2$ | $d_{cM} = 1 + 2.10\left(\frac{L}{D}\right) + 8.53\left(\frac{L}{D}\right)^2$ |
| | Dense | $d_{cM} = 1 + 3.71\left(\frac{L}{D}\right) + 4.15\left(\frac{L}{D}\right)^2$ | $d_{cM} = 1 + 2.12\left(\frac{L}{D}\right) + 10.95\left(\frac{L}{D}\right)^2$ |

displacement to a combination of horizontal and rotational deformations, especially when the aspect ratio increases. Nevertheless, the rotational mechanism observed in terms of pure horizontal loading was related to the lateral strength of soil acting on inside and outside the bucket skirt and the associated ultimate horizontal soil reaction acting normal to the loading direction. For the rough bucket foundation at high aspect ratios, circumferential shear strengths provided considerable bearing capacity to the bucket rotation and a scoop-slide mechanism was mobilized under pure horizontal loads. For low aspect ratios, the point of rotation is found to be located beneath the bucket foundation, depending on the soil-skirt roughness. In the case of the smooth interface with a high aspect ratio, the rotation point position of the laterally loaded bucket foundation moves upward from the foundation tip towards approximately 0.8 l.

With increasing relative density, the rotation center moves upward at a high aspect ratio. By comparison between sands with different relative densities, it can be observed that in the loose sand, the foundation rotates along a center of rotation deeper than that for the dense sand. It should be acknowledged that in the case of low embedment ratios ($L/D \leq 0.25$), the passive soil resistance is not noticeable, and a lower horizontal load is needed to reach failure, resulting in a larger sliding movement.

Soil-skirt roughness does significantly affect the mobilized capacities for different aspect ratios. Figure 8 outlines pure horizontal capacities versus $L/D$ at $D = 12$ m and 16 m for both rough and smooth interfaces. Figure 9 illustrates pure horizontal capacity depth factors ($d_{cH} = H_{ult(L/D)}/H_{ult(L/D=0)}$) with respect to the roughness. The FE results indicated that pure horizontal capacity depth factors can be described by linear expressions as shown in Table II. The effect of relative density and soil-skirt roughness is apparent. Higher roughness results in mobilization of higher horizontal bearing capacity depth factors. A closer inspection indicates that soil-skirt roughness could have more effects on horizontal capacity depth factors rather than vertical items.

## VI. MOMENT CAPACITY

Moment loading is worth consideration in wind turbines, which are tall and slender structures and as a result susceptible to overturn due to the eccentricity of loading. The wind at the top of the tower can produce huge moments for the bucket foundation to bear compared to

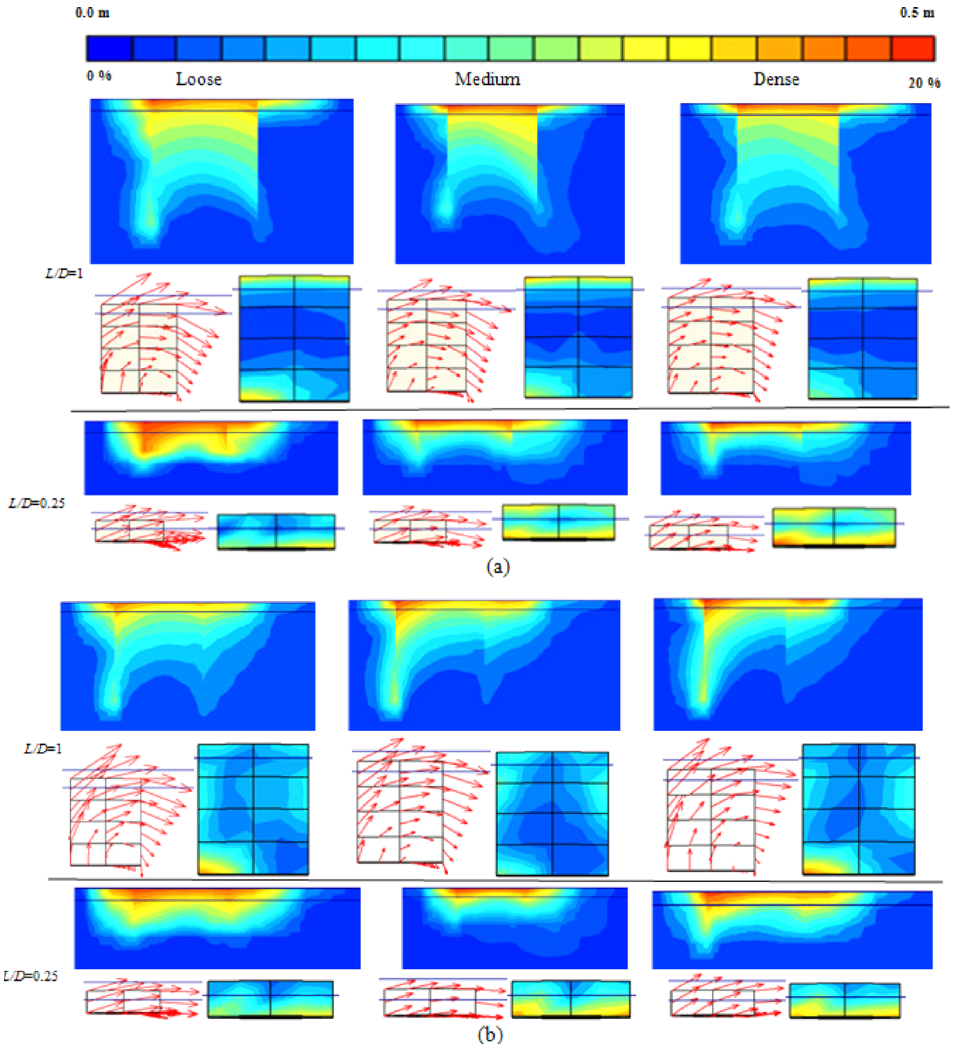


FIG. 7. Comparison of the deformation mechanisms under pure horizontal loading: (a) smooth interface and (b) rough interface.

vertical and horizontal loading imposed on it. Figure 10 shows the view of displacement vectors and plastic strain distributions under pure moment loading for smooth and rough interfaces at $D = 16$ m for $L/D = 0.25$, 1.

Under pure moment loading conditions, the failure of a surface foundation would occur due to the rotation of a scoop of the soil beneath the foundation. As a result, failure modes were found to be caused by rotation around a point located in the deformable soil plug.

A pure rotation would not accompany large deformations under pure moment due to a combination of horizontal and rotational degrees of freedom causing horizontal and rotational deformations. Parametric studies also indicate that for the lowest aspect ratio, the deformation mechanism is the type of wedge-scoop-wedge mechanism. With increasing embedment, a scoop-slide mechanism was observed under pure moment loads at the rough interface.

The discrepancy in deformation mechanisms between the smooth and rough interfaces at large aspect ratios was noticeable. Sidewalls of the bucket foundation with a smooth interface receive a negligible contribution of the moment loading, and thus, a considerable part of the bearing capacity transfers to the bucket tip level. This results in an internal scoop mechanism for the smooth interface, which leads to reduced moment bearing capacity.

For high aspect ratios under pure moment loading, the point of rotation at failure is located inside the bucket and approximately at 0.71 from the skirt lid level in the direction of the

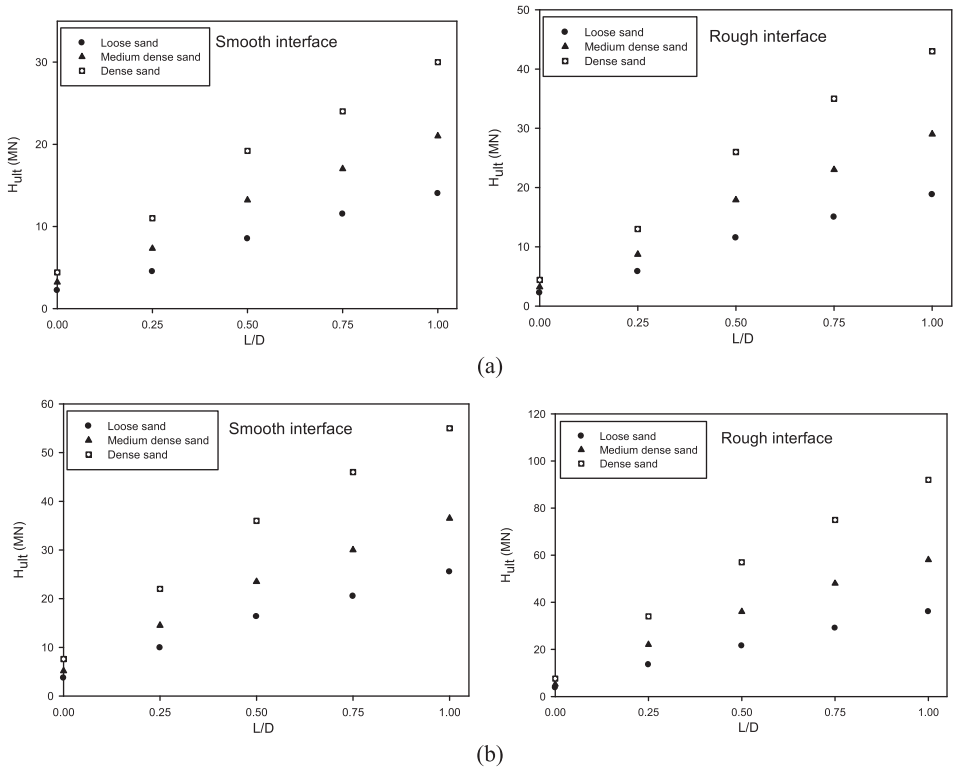


FIG. 8. Pure horizontal capacities versus aspect ratios in sands with different relative densities for smooth and rough interfaces: (a) $D = 12$ m and (b) $D = 16$ m.

loading. In the case of the low aspect ratio, the rotation center may locate inside the foundation but not always, highly dependent on the relative density like that predicted in denser soil bodies, where the center of rotation transfers to shallower depths rather than loose deposits. Interestingly, an increase in the load eccentricity is found to move the point of rotation upward. It was found that the assumption of soil behavior confined within the bucket foundation as a rigid cluster during moment loading would lead to the overestimation of the moment bearing capacity.

Figure 11 compares pure moment capacities between different sand types in both smooth and rough bucket foundations.

All smooth bucket foundations indicated lower moment capacities than the rough ones. It would not seem to be conservative to assume a roughness of zero for the skirt compartment of the bucket foundation. Roughness had more effects on pure moment capacity of the bucket foundation compared to pure vertical and horizontal capacities. The pure moment capacity was larger in dense sand than medium and loose sands. When the degree of embedment increases, the difference will become greater.

Figure 12 also shows pure moment capacity depth factors ($d_{cM} = M_{ult(L/D)}/M_{ult(L/D=0)}$) dependent upon aspect ratios for smooth and rough bucket foundations with varying sand profiles.

## VII. BEARING STRENGTH ENVELOPES

For the purpose of identifying the effect of the vertical load on normalized envelopes in load space $H/H_{ult}$, a campaign of vertical load levels of $V = 0$, $0.2V_{ult}$, $0.3V_{ult}$, $0.5V_{ult}$, $0.7V_{ult}$, $0.9V_{ult}$, $0.95V_{ult}$, and $V_{ult}$ is considered. The vertical load was kept constant through the FE analyses like offshore sites where the vertical load accounts for the weight of superstructure itself as well as foundation. Figure 13 illustrates the normalized uniaxial load-carrying

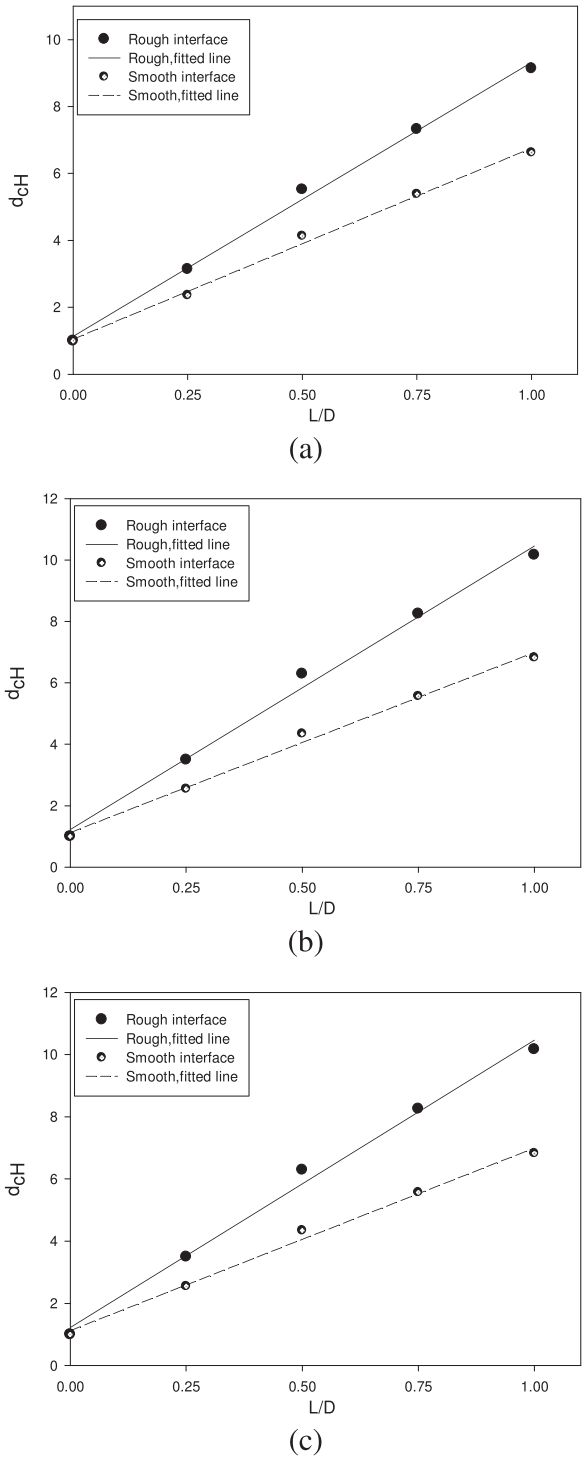


FIG. 9. Comparison of Pure horizontal capacity depth factors between smooth and rough bucket foundations: (a) loose sand, (b) medium sand, and (c) dense sand.

capacities resulting from the FE analyses with respect to the level of vertical loading and soil-skirt roughness in medium-dense sand for $L/D = 0.5$, 1. It is observed that until a distinct vertical load level of $0.5V_{ult}$, the uniaxial bearing capacities show an increase owing to capacity mobilization with the combination of horizontal and rotational translations in $H = H_{ult}$, which is

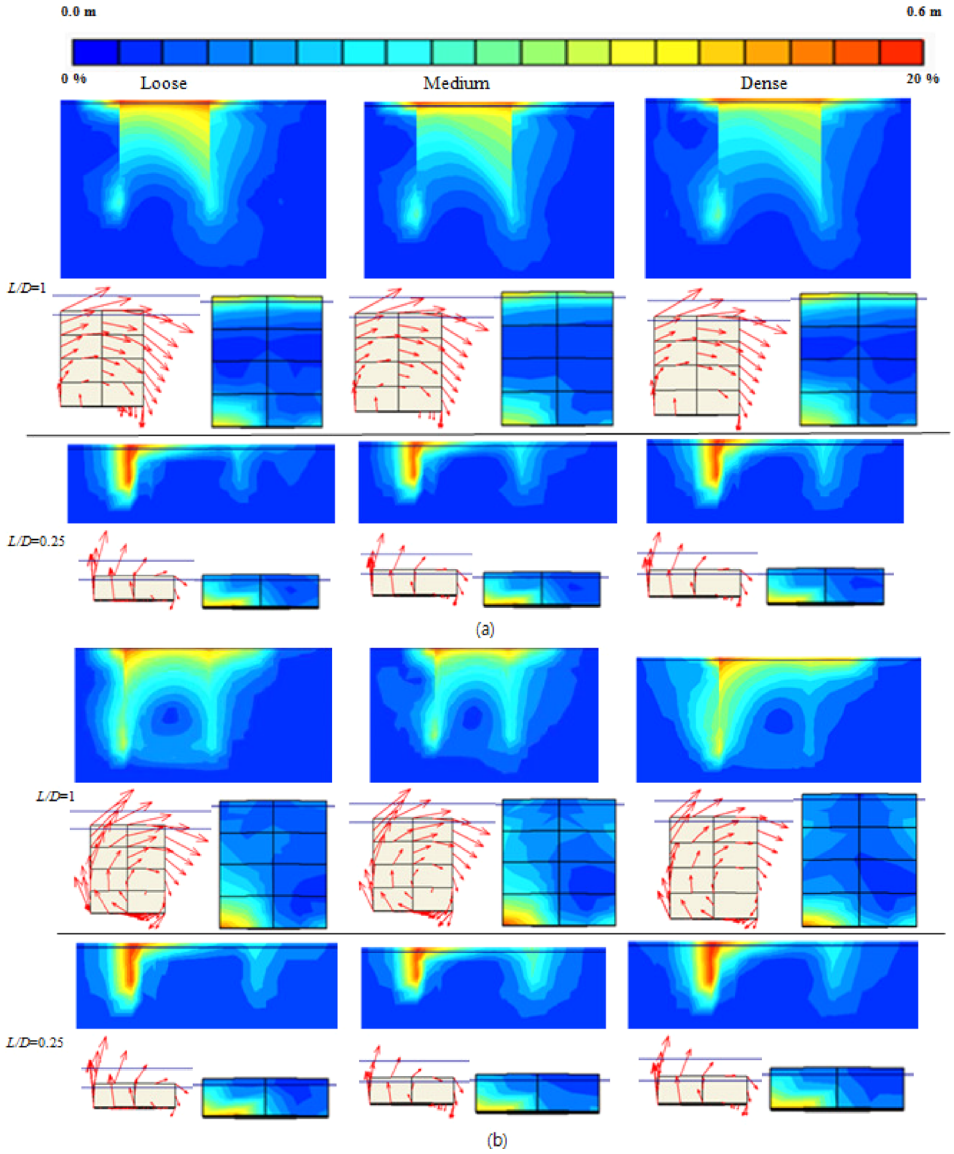


FIG. 10. Comparison of the displacement vectors and plastic strain distributions under pure moment loading: (a) smooth interface and (b) rough interface.

reversed at higher vertical load levels until failure is achieved. In the *VH* load space, with the increasing aspect ratio, concavity of failure envelopes reduces and shifts towards the flat shape since contribution of the tip of the bucket to bearing capacity started to disappear. The effect of roughness on the bearing capacity for larger aspect ratios ($L/D = 1$) was less than lower embedment.

Failure envelopes in *VH* load space ($M = 0$) can be expressed in terms of normalised horizontal and vertical loads as

$$h' = (av^2 + bv + 1)^c (1 - v)^d, \tag{5}$$

where $h' = H/H_{ult}$ and $v = V/V_{ult}$. Table III shows constants fitted into Eq. (5) for different aspect ratios and interface roughness values.

Interaction diagrams under combined vertical and moment loading predicted by the finite element analyses in *VM* ($H = 0$) load space are presented in Fig. 14 for the range of aspect

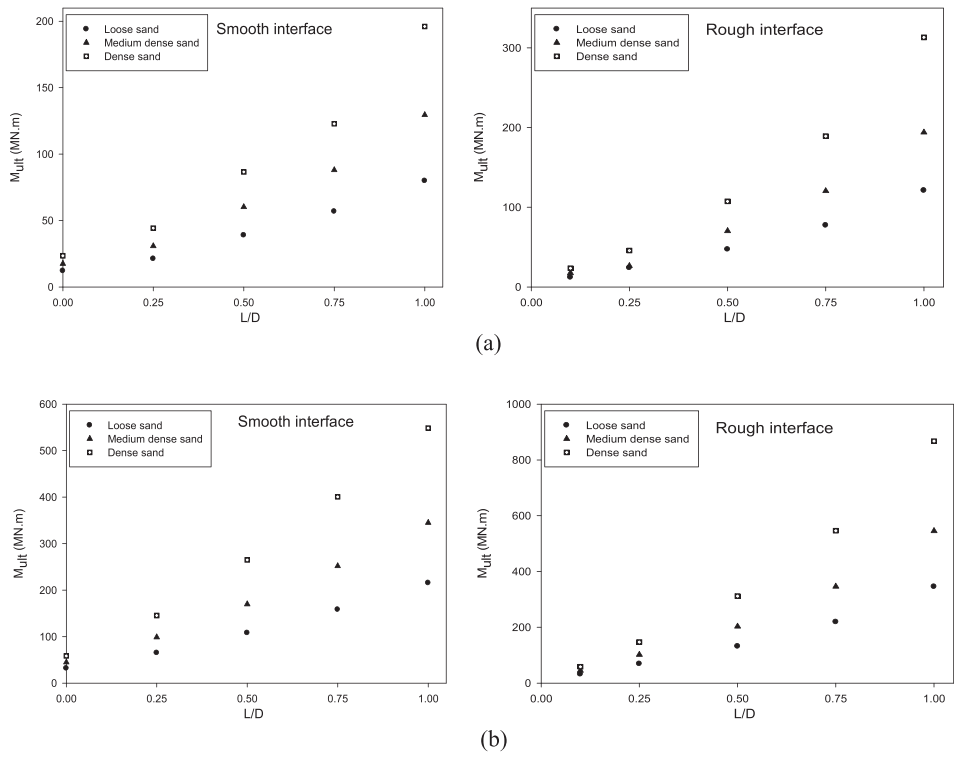


FIG. 11. Pure moment capacities versus aspect ratios in loose, medium, and dense sands for smooth and rough interfaces: (a) $D = 12$ m and (b) $D = 16$ m.

ratios, soil–skirt interface conditions, and level of vertical mobilization in medium-dense sand. The ultimate moment increases with the increasing vertical load level in an almost linear manner for $V \leq 0.5V_{ult}$. By contrast for $V > 0.5V_{ult}$, moment capacity decreases with the increasing level of vertical loading. Hence, the failure mechanism $VM$ load space is highly dependent on the interaction of moment with the applied vertical load. It must be noted that concavity in the normalized bearing capacity curves $M/M_{ult}$ against $V/V_{ult}$ increase with reducing embedment for both the smooth and rough interfaces. It may be attributed to the alteration of the failure mechanism, which is due to the fact that with increasing embedment, sidewall resistance will raise and delay the mobilization of the bucket capacity in the tip level. At aspect ratio $L/D = 1$, capacity dependency to roughness was lower than $L/D = 0.5$.

In order to determine normalized moment and vertical capacities in $VM$ load space ($H = 0$), the following expression is derived:

$$m' = (av^2 + bv + 1)^c (1 - v)^d, \tag{6}$$

where $m' = M/M_{ult}$ and $\nu = V/V_{ult}$. Table IV presents coefficients fitted into Eq. (6) for rough and smooth interfaces at $L/D = 0.5$, 1.

## VIII. CONCLUSIONS

This study investigated the results of three-dimensional numerical analyses of smooth and rough interface bucket foundations found at densities of interest under uniaxial loads. The influence of variations in the geometry of the bucket (length-to-diameter aspect ratio $L/D$), soil-foundation interface roughness, soil type and level of vertical mobilisation on pure bearing capacity was evaluated and discussed. As such, they were all found to be significantly important in capturing the capacities of bucket foundations.

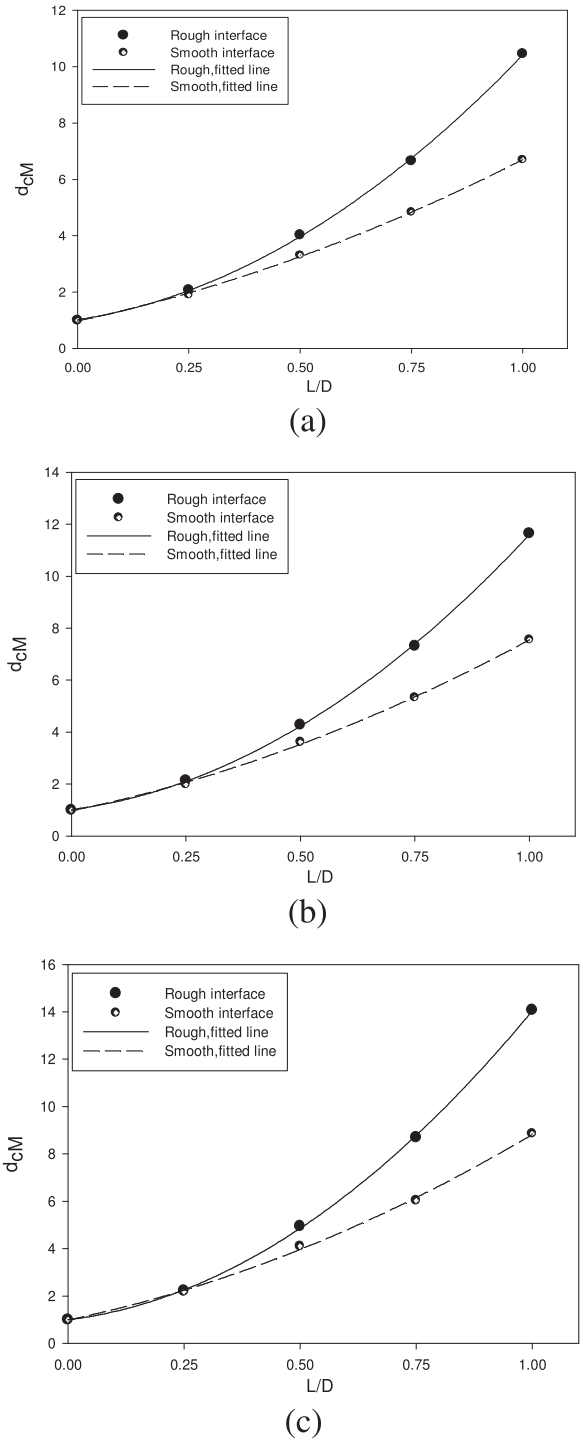


FIG. 12. Comparison of pure moment capacity depth factors between smooth and rough bucket foundations: (a) loose sand, (b) medium sand, and (c) dense sand.

In general, embedment increased uniaxial capacities at various soil and soil-foundation interface conditions as failure mechanisms were forced deeper within the soil mass. The vertical skirts under the bed interacted with the soil and caused pure vertical, horizontal, and moment bearing capacities to increase, compared to the surface foundation. Sidewalls in bucket foundations are proved to play an important role in soil-bucket foundation response

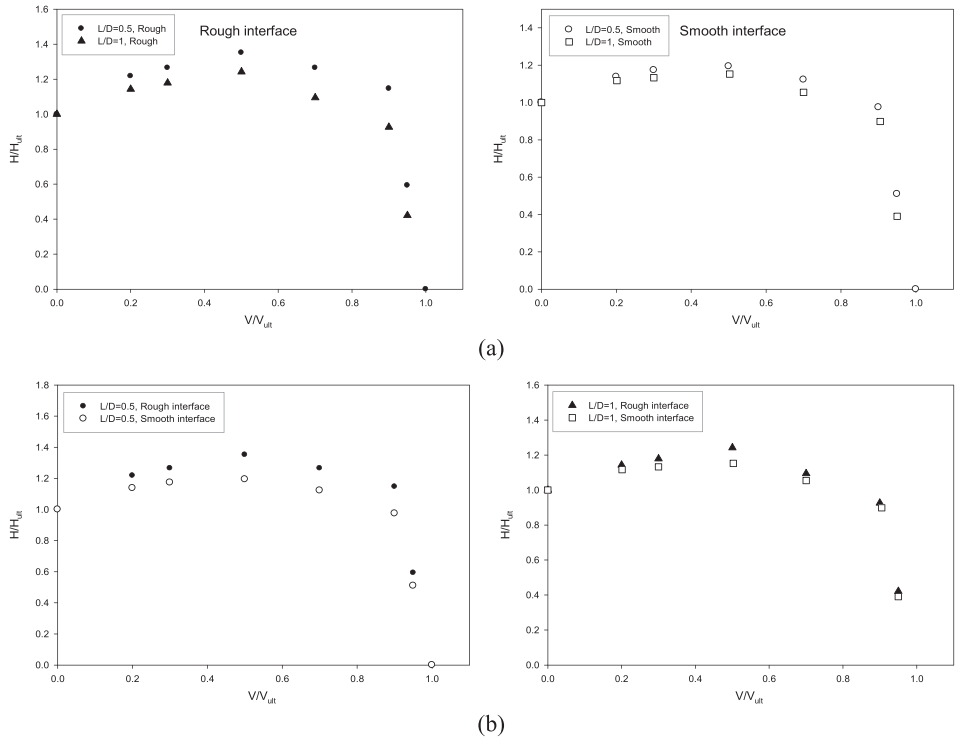


FIG. 13. Normalised failure envelopes in *VH* load space ($M = 0$): (a) embedment effect and (b) roughness effect.

to uniaxial loads, being able to transfer them through normal and shear stresses to the surrounding soil.

The mechanism of failure under pure loading of bucket foundations was supposed to be less dependent on the bucket diameter but much more on the embedment, soil-skirt interface roughness, and sand types. Failure under the pure horizontal load and moment was governed by a combination of horizontal and rotational translations unlike pure vertical capacity in which failure was roughly governed by settlement. The results showed that the discrepancy in the shape of failure mechanisms between two interface assumptions (smooth and rough) was large at different aspect ratios.

Smooth bucket foundations result in lower uniaxial bearing capacities compared to the rough interface for all aspect ratios and soil types investigated. For the Smooth bucket foundation, the sidewall does not sufficiently contribute to load transition, and hence, a significant part of the uniaxial loads was assigned to the bucket tip level, which resulted in the decreasing rate of bearing capacity as the interface coefficient decreases.

Depth factors of pure horizontal and vertical bearing capacities were found to be proportional to aspect ratios linearly, while a quadratic relationship was observed between the aspect ratio and the pure moment capacity depth factor.

In the case of failure envelopes in horizontal ($H/H_{ult}$) load space against $V/V_{ult}$, normalised horizontal capacity increases with the increasing vertical load for $V \leq 0.5V_{ult}$. By contrast, the

TABLE III. Constants in Eq. (5) for different aspect ratios and interface coefficients.

| *L/D* | Roughness | *a* | *b* | *c* | *d* |
|---|---|---|---|---|---|
| 0.5 | Rough | 0.01 | 0.12 | 10.98 | 0.56 |
| 0.5 | Smooth | 0.01 | 0.05 | 22.62 | 0.59 |
| 1 | Rough | 0.01 | 0.07 | 18.23 | 0.66 |
| 1 | Smooth | 0.01 | 0.03 | 35.68 | 0.69 |

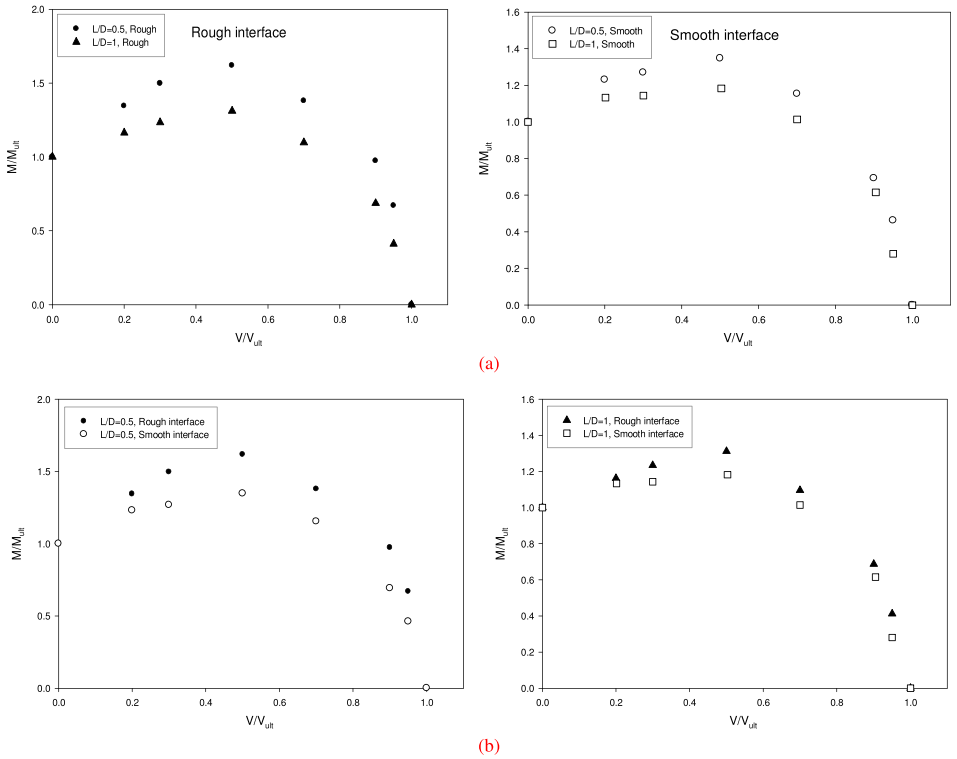


FIG. 14. Normalised failure envelopes in *VM* load space ($H = 0$): (a) embedment effect and (b) roughness effect.

TABLE IV. Constants related to Eq. (6) for rough and smooth interfaces at $L/D = 0.5, 1$.

| *L/D* | Roughness | *a* | *b* | *c* | *d* |
|---|---|---|---|---|---|
| 0.5 | Rough | −0.51 | 0.79 | 3.06 | 0.38 |
| 0.5 | Smooth | −0.15 | 0.38 | 4.87 | 0.59 |
| 1 | Rough | 32.9 | 1.43 | 0.30 | 0.62 |
| 1 | Smooth | 0.02 | 0.15 | 9.96 | 0.87 |

inverse behaviour is observed for vertical loads higher than $0.5V_{ult}$, whose horizontal capacity diminishes with the increasing level of vertical loading for both smooth and rough interfaces. As the embedment increases, curves of normalised failure envelopes shift from the concave shape to the flat shape. In *V-M* load space, normalized moment capacity is mobilized in conjunction with a vertical load level approximately half the uniaxial bearing capacity, and for vertical load levels bigger than $0.5V_{ult}$, normalized moment capacity decreases.

The depth factor relationships were suggested according to the results achieved by parametric studies. The presented curves and functions could be utilized in a preliminary design and engineering practice to evaluate appropriate bucket dimensions.

Achmus, M., Akdag, C. T., and Thieken, K., "Load-bearing behavior of suction bucket foundations in sand," Appl. Ocean Res. **43**, 157–165 (2013).

American Petroleum Institute (API), *Recommended Practice for Planning, Designing and Constructing Fixed Offshore Platforms- Working Stress Design 2A-WSD*, 21st ed. (American Petroleum Institute, 2002).

Barari, A. and Ibsen, L. B., "Undrained response of bucket foundations to moment loading," Appl. Ocean Res. **36**, 12–21 (2012).

Barari, A. and Ibsen, L. B., "Insight into the lateral response of offshore shallow foundations," Ocean Eng. **144**(1), 203–210 (2017).

Barari, A., Ibsen, L. B., Taghavi, A., and Larsen, K. A., "Embedment effects on the vertical bearing capacity of offshore bucket foundations on cohesionless soil," Int. J. Geomech. **17**(4), Article number 04016110 (2017).
Bienen, B., Gaudin, C. H., Cassidy, M., Rausch, L., and Purwana, O. A., "Numerical modeling of undrained capacity of hybrid skirted foundation under combined loading," Int. J. Offshore Polar Eng. **22**(4), 323–329 (2012).
Bransby, M. and Randolph, M. F., "Combined loading of skirted foundations," Geotechnique **48**(5), 637–655 (1998).
Bransby, M. F. and Yun, G. J., "The undrained capacity of skirted strip foundations under combined loading," Geotechnique **59**(2), 115–125 (2009).
Byrne, B. W. and Houlsby, G. T., "Drained behavior of suction caisson foundations on very dense sand," in *Offshore Technology Conference*, OTC 10994 (1999).
Delft University of Technology, Netherlands, *User's Manual*, Version 1.6 (Delft University of Technology, 2005).
DNV, "Foundations, classification notes," No. 30.4, Det Norske Veritas Classification A/S, February 1992.
Foglia, A., Ibsen, L. B., Nielsen, S. K., and Mikalauskas, L., "A preliminary study on bucket foundations under transient lateral loading," in *Proceedings of the 23rd International Offshore and Polar Engineering Conference* (2013), Vol. 2.
Gerolymos, N, Zafeirakos, A., and Souliotis, C., "Insight to failure mechanisms of caisson foundations under combined loading: A macro-element approach," in *Second International Conference on Performance-Based Design in Earthquake Geotechnical Engineering*, Taormina, Italy (2012).
Gourvenec, S., "Failure envelopes for offshore shallow foundations under general loading," Geotechnique **57**(9), 715–728 (2007).
Gourvenec, S., "Effect of embedment on the undrained capacity of shallow foundations under general loading," Géotechnique **58**(3), 177–185 (2008).
Gourvenec, S. and Randolph, M., "Effect of strength non-homogeneity on the bearing capacity of circular skirted foundations subjected to combined loading," in *Proceedings of the Twelfth International Offshore and Polar Engineering Conference*, Kitakyushu, Japan (2002).
Gourvenec, S. and Randolph, M., "Bearing capacity of a skirted foundation under VMH loading," in *Proceedings of OMAE03 22nd International Conference on Offshore Mechanics and Arctic Engineering*, Cancun, Mexico (2003).
Houlsby, G. T., Ibsen, L. B., and Byrne, B. W., "Suction caissons for wind turbines," in *Proceedings of the Frontiers in Offshore Geotechnics* (ISFOG 2005), University of Western Australia, Perth (2005).
Ibsen, L., "Implementation of a new foundation concept for offshore wind farms," in *Norsk Geoteknisk Forening*, Keynote, NGM (2008).
Ibsen, L. B., Barari, A., and Larsen, K. A., "Modified vertical bearing capacity for circular foundations in sand using reduced friction angle," Ocean Eng. **47**, 1–6 (2012).
Ibsen, L. B., Barari, A., and Larsen, K. A., "Adaptive plasticity model for bucket foundations," J. Eng. Mech. **140**(2), 361–373 (2014a).
Ibsen, L. B., Barari, A., and Larsen. K. A., "Effect of embedment on the plastic behaviour of bucket foundations," J. Waterw., Port, Coastal, Ocean Eng. **141**(6), Article number 06015005 (2015).
Ibsen, L. B., Larsen, K. A., and Barari, A., "Calibration of failure criteria for bucket foundations on drained sand under general loading," J. Geotech. Geoenviron. Eng. **140**(7), Article number 04014033 (2014b).
ISO (International Standardisation Organisation), *ISO 19901-4: Petroleum and Natural Gas Industries—Specific Requirements for Offshore Structures—Part 4: Geotechnical and Foundation Design Considerations*, 1st ed. (International Standardisation Organisation, Geneva, Switzerland, 2003).
Jalbi, S., Shadlou, M., and Bhattacharya, S., "Impedance functions for rigid skirted caissons supporting offshore wind turbines," Ocean Eng. **150**, 21–35 (2018).
Larsen, K. A., Ibsen, L. B., and Barari, A., "Modified expression for the failure criterion of bucket foundations subjected to combined loading," Can. Geotech. J. **50**(12), 1250–1259 (2013).
Liu, M., Lian, J., and Yang, M., "Experimental and numerical studies on lateral bearing capacity of bucket foundation in saturated sand," Ocean Eng. **144**, 14–20 (2017).
Liu, R., Chen, G., Lian, J., and Ding, H., "Vertical bearing behavior of the composite bucket shallow foundation of offshore wind turbines," J. Renewable Sustainable Energy **7**, 013123 (2015).
Mana, D. S. K., Randolph, M. F., Gourvenec, S. M., and Hossain, M. S., "Failure mechanisms of skirted foundations in uplift and compression," Int. J. Phys. Modell. Geotech. **12**(2), 47–62 (2012).
Park, J. S., Park, D., and Yoo, J. K., "Vertical bearing capacity of bucket foundations in sand," Ocean Eng. **121**, 453–461 (2016).
Salgado, R., Lyamin, A. V., Sloan, S. W., and Yu, H. S., "Two and three-dimensional bearing capacity of foundations in clay," Géotechnique **54**(5), 297–306 (2004).
Vesic, A., "Bearing capacity of deep foundations in sand," Highw. Res. Rec. **39**, 112–153 (1963).
Vesic, A., "Analysis of ultimate loads of shallow foundations," ASCE J. Soil Mech. Found. Div. **99**(SM1), 45–73 (1973).
Vulpe, C., "Design method for the undrained capacity of skirted circular foundations under combined loading: Effect of deformable soil plug," Géotechnique **65**(8), 669–683 (2015).
Wang, X., Yang, X., and Zeng, X., "Lateral capacity assessment of offshore wind suction bucket foundation in clay via centrifuge modeling," J. Renewable Sustainable Energy **9**, 033308 (2017).
Yun, G. and Bransby, M. F., "The undrained vertical bearing capacity of skirted foundations," Soils Found. **47**(3), 493–505 (2007).
Zafeirakos, A. and Gerolymos, N., "Bearing strength surface for bridge caisson foundations in frictional soil under combined loading," Acta Geotech. **11**, 1189–1208 (2016).
Zhang, P., Xiong, K., Ding, H., and Le. C., "Anti-liquefaction characteristics of composite bucket foundations for offshore wind turbines," J. Renewable Sustainable Energy **6**(5), 053102 (2014).
Zou, X., Hu, Y., Hossain, M. S. H., and Zhou, M., "Capacity of skirted foundations in sand-over-clay under combined V-H-M loading," Ocean Eng. **159**, 201–218 (2018).